Optics & Laser Technology 174 (2024) 110619

Contents lists available at ScienceDirect

Optics and Laser Technology

journal homepage: www.elsevier.com/locate/optlastec

Full length article

Ultrafast thermalization dynamics in silicon wafer excited by femtosecond laser double-pulse vortex beam

Guangqing Du, Fangrui Yu, Ahmad Waqas, Feng Chen *

State Key Laboratory for Manufacturing System Engineering and Shaanxi Key Laboratory of Photonics Technology for Information, School of Electronic Science and Engineering, Xi'an Jiaotong University, Xi'an 710049, PR China

ARTICLE INFO

Keywords:
Thermalization dynamics
Double-pulse
Vortex beam
Nonequilibrium state

ABSTRACT

The ultrafast thermalization dynamics of silicon wafers excited by a femtosecond laser double-pulse vortex beam was theoretically investigated via multi-physical fields simulations. A self-consistent model was developed, which comprehensively considers for the transient properties of optical, electronic and thermal parameters to predict the vortical thermalizations in silicon wafers. The spatial-temporal evolutions for carrier density and vortical temperature fields in nonequilibrium state of photo-excited silicon wafer are obtained in details. It is revealed that the photo-generated carrier can be significantly multiplied by utilizing a femtosecond laser double-pulse vortex beam, simultaneously amplifying the vortical thermalization dynamics of silicon wafer. The results can be attributed to two factors of the enhanced light absorption and the amplified carrier-phonon coupling dynamics via double-pulse vortex beam excitations. The results can provide for basic insights into the vortical heating dynamics of femtosecond laser double-pulse vortex beam interactions with semiconductors, putting forward the feasibility of advanced vortex beam applications for STED imaging, ultrafast SERS sensing and laser fabrication of sophisticated structures, etc.

1. Introduction

In past years, there has been significant progress in the study of Femtosecond (fs) laser interactions with silicon wafers with a focus on understanding advanced carrier dynamics for both academic and practical purposes [1–7]. When a femtosecond laser interacts with a silicon target, it triggers non-linear ionization and subsequent thermalization dynamics in a highly non-equilibrium state where carriers and phonons are locally decoupled in photo-excited silicon [8–11]. This presents opportunities for achieving high-precision machining of silicon targets by potentially avoiding Fourier thermal diffusion during the dynamically decoupling period that typically occurs on the femtosecond to picosecond timescales.

Recently, advancements in topology-structured light in the form of non-Gaussian profiles with phase-controlled wave front can provide for even more flexible route for potential applications of advancing nanomanufacturing, super-resolution imaging and molecular spectroscopy. [12–16]. One specific type of this light, optical vortex beam (OVB) which carries a helical phase wave front and annular intensity profile offers unique opportunities for controlling light-matter interactions. Nivas et al. experimentally demonstrated the flexibility of controlling surface ripple properties using optical vortex beam compared to Gaussian beams [17]. By tuning the topological charge of the vortex beam phase, the transition of the ablation crater between sub-wavelength ripples and holes, as well as the switching of ripple orientation are experimentally observed by Zhao et al. [18]. On the other hand, it is often reported that using a femtosecond laser double-pulse beam allows for more precise control of materials ablation with high flexibility [19–22]. In particular, controlling of the thermal dynamics of laser material interactions is essentially important for advancing the potential applications of laser ablation, ultrafast resolution imaging and SERS sensing. Therefore, manipulating the vortical thermalization dynamics in a silicon wafer with a femtosecond laser double-pulse vortex beam can be of crucial importance for exploring the exceptional merit of flexible and high-precision processing of silicon targets for specific applications of topology-structured light. However, there is still a challenge in fully exploring the particular vortical thermalization dynamics in highly nonequilibrium states of silicon wafers owing to the complex coupled thermal transfer dynamics with respect to the topology-structured vortex beam irradiation. Therefore, gaining a

* Corresponding author.
E-mail address: chenfeng@mail.xjtu.edu.cn (F. Chen).

https://doi.org/10.1016/j.optlastec.2024.110619
Received 28 July 2023; Received in revised form 1 December 2023; Accepted 12 January 2024
Available online 19 January 2024

comprehensive understanding of the thermalization dynamics of photo-excited silicon wafers by a femtosecond laser double-pulse vortex beam is crucial for advancing applications such as vortex beam nano-manufacturing, super-resolution imaging, and SERS sensing etc. To the best of our knowledge, the vortical thermalization dynamics in silicon wafers under femtosecond laser double-pulse vortex beam irradiation have not been thoroughly explored.

In this paper, we present theoretical investigations on the ultrafast thermalization dynamics in silicon with respect to carrier generation, relaxation and accompanying vortical thermalization when exposed to femtosecond double-pulse vortex beams. We have built a self-consistently coupled dynamic model, that fully considers the complicatedly coupled dynamics of electronic and thermal modifications in a photo-excited silicon wafer following femtosecond laser double-pulse vortex beam irradiation. Our findings reveal that the second pulse of the double-pulse configuration plays a significant role in facilitating the coupling of laser energy into the silicon wafer, resulting in an elevated vortical temperature field on a sub-picosecond timescale. Additionally, the amplified carrier-phonon coupling dynamics can well explain the intensified energy coupling dynamics in silicon wafers especially at higher fluence levels after irradiation with double-pulse vortex beams.

2. Modelling and methods

The complex amplitude of a laser vortex beam with a topological charge l can be well described by [23,24]

$$\widetilde{U}(r,z) = A_0 c\left(\frac{r\sqrt{2}}{w(z)}\right)^{l}\exp\left[\frac{-r^2}{w^2(z)}\right]\bullet\exp\left[i\frac{kr^2}{2R}\right]\bullet\exp[il\theta]\bullet\exp[i\phi(z)] \tag{1}$$

Where, A_0 is the physical amplitude of incident light field, w denotes the radius of vortex beam spot, c is a scalable normalization factor, $w(z) = w_0\sqrt{1+z^2/z_R^2}$, with $z_R = \frac{\pi w^2}{\lambda}$denoting the Rayleigh distance. w_0 is the waist radius of the fundamental Gaussian beam. θ is the polar angle in circumferential direction of the vortex beam. The Gouy phase is defined as $\phi(z) = \arctan(z/z_R)$, where R is the wave front curvature radius of the vortex beam. r represents the radius of polar coordinate at the focusing plane ($z = 0$), and l denotes topological charge of vortex beam. In this simulation, we assume the temporal shape-invariant of the femtosecond pulse intensity which can produce fundamental results compared to solving the Helmholtz equation for the complex amplitude of laser electric field, while saving computation time. We are using a femtosecond laser vortex beam with a Gaussian temporal envelope, represented by the equation $I(r,z,t) = \left|\widetilde{U}\right|^2\exp\left[-4\ln2\left(\frac{t-2t_p}{t_p}\right)^2\right]$, where t_p is the pulse duration defined by full width at half maximum (FWHM). In this work, the femtosecond laser double-pulse vortex beam refers to two aspects of pulse shaping: considering the spatial profile in the vortex beam and the temporal profile in term of a delayed double-pulse. Therefore, the intensity of the femtosecond laser double-pulse vortex beam with a topological charge l can be described in the form of pulse fluence, written as

$$I = \sqrt{\frac{4\ln(2)}{\pi}}\left(\frac{e}{l}\right)^{l}\left(\frac{r\sqrt{2}}{w_0}\right)^{2l}\exp\left[\frac{-2r^2}{w_0^2}\right]\cdot \sum_{i=1}^{2}\frac{F_i}{t_{pi}}\exp\left[-4\ln2\left(\frac{t-2t_{pi}-(i-1)\Delta}{t_{pi}}\right)^2\right] \tag{2}$$

Here, F_i and t_{pi} denote the fluence and pulse duration for i*th* pulse of double-pulse vortex beam, respectively. Δ represents the temporal separation of femtosecond laser double-pulse vortex beam.

The transient dielectric function for excited silicon can be mathematically written as follows [25]:

$$\varepsilon_{si} = 1 + \left(\varepsilon_g(\omega) - 1\right)\left(\frac{N_v - N}{N_v}\right) - \frac{n_e e^2}{\omega^2}\left[\frac{1}{m_e^*(1 + i\nu_{coll.}/\omega)} + \frac{1}{m_h^*(1 + i\nu_{coll.}/\omega)}\right] \tag{3}$$

The dielectric function of unexcited silicon, $\varepsilon_g(\omega)$ depends on the laser wavelength, N_v is the carrier density in the valence band which is taken as 5×10^{22} cm^{-3} for silicon, N denotes the number density of the photogenerated carrier in the conduction band, and ω is the laser angular frequency. In the highly non-equilibrium state of photo-excited silicon, the Drude collision frequency $\nu_{coll.}$ can be phenomenologically defined as an identical value for effective carriers and holes by introducing the effective optical mass, written as $1/m_{opt}^* = 1/m_e^* + 1/m_h^*$. Here, m_e^* and m_h^* denote the effective mass of the carrier and hole. By applying Fresnel's law to the excited silicon surface, we can obtain the carrier density-dependent reflectivity as follows:

$$R_{si} = \frac{\left[Re\left(\sqrt{\varepsilon}\right) - 1\right]^2 + [Im(\sqrt{\varepsilon})]^2}{\left[Re\left(\sqrt{\varepsilon}\right) + 1\right]^2 + [Im(\sqrt{\varepsilon})]^2} \tag{4}$$

The dynamic processes of transient non-linear light absorption and the carrier generation in silicon can be written as follows [26,27]:

$$\nabla I\cdot\vec{n} = \left(\alpha\ I + \beta I^2\right) + \alpha_f I \tag{5}$$

$$\frac{\partial N}{\partial t} = \nabla\cdot\vec{J} + G\frac{N_v - N}{N_v} - R \tag{6}$$

Where, I denotes the laser intensity of the vortex beam, and $\vec{n}$ is the inward normal vector at the front surface of silicon target. α, β and α_f are the coefficients for one-photon absorption, two-photon ionization and free carrier absorption, respectively. Here, α_f is the transient dielectric function for fully ionized silicon in the skin layer, which can be evaluated for $N = N_v$, written as $\alpha_f = \frac{2\omega}{c}Im(\varepsilon_{Si})$. The carrier current can be written as $\vec{j} = D_0(\nabla N)$. Where D_0 denotes the temperature-dependent carrier ambipolar diffusivity. The term$G = \frac{\alpha I}{\hbar\omega} + \frac{\beta I^2}{2\hbar\omega} + \delta_I N$accounts for the carrier generation rate due to single photon, two-photon and impact ionization, respectively. The term $R = N\left[\tau_{AR} + (C_{AR}N^2)^{-1}\right]^{-1}$ describes the carrier loss rate due to the Auger recombination, with τ_{AR} and C_{AR} representing Auger recombination time and rate, respectively.

The silicon wafer is initially ionized by the first vortex pulse in femtosecond laser double-pulse vortex beam irradiation, creating the nonequilibrium state in the ionized region. When the second vortex pulse reaches the surface of the pre-ionized silicon, it dynamically interacts with the pre-ionized state. After the double-pulse vortex beam irradiation, the vortical thermalization dynamics are dominated by two-temperature processes until the carrier and phonon reach thermal equilibrium in the photo-ionized region of silicon. The dynamics of silicon at two-temperatures state following femtosecond double-pulse vortex beam irradiation can be mathematically described by [28]

$$C_c\frac{\partial T_c}{\partial t} = \nabla(k_c\nabla T_c) - \gamma\left(T_c - T_p\right) + S \tag{7}$$

$$C_p\frac{\partial T_p}{\partial t} = \nabla\left(k_p\nabla T_p\right) + \gamma\left(T_c - T_p\right) \tag{8}$$

Where, the carrier thermal capacity is approximately calculated as $C_c = \frac{\partial[NE_g + 3/2Nk_BT_c]}{\partial T_c} = \frac{3}{2}Nk_B$ in the highly nonequilibrium state for photo-excited silicon. The carrier thermal conductivity k_c depends on both the density and temperature of the carrier system, and is defined by $k_c = 2k_B^2\mu_e NT_c/e$. The carrier-phonon coupling factor is calculated by $\gamma = C_c/\tau_{c-p}$, with $\tau_{c-p} = \tau_0[1 + (N/N_{cr})]$. The phonon thermal capacity is considered as a temperature-dependent parameter, written by$C_p = 10^6$

$\times$ [1.978+(3.54 $\times$ 10^{-4})T_p −3.68T_p^{-2}]. Here, the phonon thermal conductivity is adopted as $k_p = 10^2 \times 1585T_p^{-1.23}$. The source term S represents the rate at which laser energy is deposited by a double-pulse vortex beam, written by [28]

$$S = \left[(\hbar\omega - E_g)\frac{\alpha I}{\hbar\omega} + (\hbar\omega - E_g)\frac{\beta I^2}{2\hbar\omega} - \delta_{II} E_g N \right] \bullet \left(\frac{N_v - N}{N_v}\right) + [\alpha_B I + E_g R] - [\frac{\partial (NE_g)}{\partial t} + \frac{3}{2}k_B T_e \frac{\partial N}{\partial t}] \quad (9)$$

Where, the first three terms account for one-photon absorption, two-photon absorption and the energy loss of electron avalanche. The middle terms $\alpha_B I$ and $E_g R$ represent the energy releases due to carrier heating and Auger recombination. The last two terms denote carrier energy changes due to transient modifications of band gap energy and carrier thermal capacity.

Due to the flexibility of the Finite Element Method (FEM), which is used to solve the coupled dynamic partial differential equations, (Eqs. (5)-(8)) in COMSOL Multiphysics. The boundary condition for the laser absorption equation (5) is represented by $(1 - R_{Si})I_{Double-pulse}|(z = 0)$ which accounts for the external laser source on the front surface of silicon. The bottom and side-wall boundaries are treated as the perfectly matching layers for the scattered light intensity. In this simulation, carrier escape and thermal losses from the silicon wafer to the external environment can be neglected on femtosecond to picosecond timescales. This allows carrier density N, carrier temperature T_c and the phonon temperature T_p to satisfy the following boundary conditions: $\nabla N \bullet \vec{n}|_\Omega = 0$, $k_c \nabla T_c \bullet \vec{n}|_\Omega = 0$, $k_p \nabla T_p \bullet \vec{n}|_\Omega = 0$.The zero laser intensity in the silicon wafer target before laser irradiation is naturally set as the initial condition. The initial condition for carrier density N is 1.5 $\times$ $10^{10} cm^{-3}$ in the unexcited state for intrinsic silicon. The initial conditions for T_c and T_p are set at 300 K which is room temperature. All parameters for silicon used in the ultrafast vortical thermalization simulations can be found in Table1.

The 2D spatial spots at the focusing plane of the femtosecond laser vortex beam with typical topological charges of 1, 2 and 3 are shown in Fig. 1. These spots were collected at the pulse peak of the double-pulse vortex beam. The 2D electric field spots in Fig. 1(a)~(c) is defined by the scalar electric field amplitude that is modulated by polar angle θ at the focusing plane of vortex beam, the maps in Fig. 1(d)~(f) is defined by the laser intensity, calculated as $|\widetilde{U}(r, z)|^2$. The electric field and laser intensity of the vortex beam are normalized for exclusive analysis of the

Table 1
The parameters of silicon employed for the simulations [25,26,29].

Quantity	Symbol	Values
One-photon absorption	α	$10^2 \cdot 1.12 \times 10^3\, e^{(T_p/430)}$ m^{-1}
Two-photon absorption	β	10×10^{-11} mW^{-1}
Boltzmann constant	k_B	$1.3806505 \times 10^{-23}$ J/K
Free-carrier mobility	μ_e	$e/(m_e \nu)$
Free-carrier collision frequency	ν	1.5×10^{14} Hz
Carrier ambipolar diffusivity	D_0	$18 \times 10^{-4} \cdot (300/T_p)$ m^2/s
Light angular frequency	ω	$2\pi c/\lambda$
Impact ionization coefficient	δ_I	$3.6 \times 10^{10}\, e^{-E_g/k_B T_c}$
Auger recombination time	τ_{AR}	6×10^{-12} s
Auger recombination rate	C_{AR}	$3.8 \times 10^{-43}\, m^6/s$
Initial coupling time	τ_0	240×10^{-15} s
Critical carrier density	N_{cr}	8.7×10^{27} m^{-3}
Band gap	E_g	1.6×10^{-19}[1.16–7.02 $\times$ 10^{-4} $T_p^2/(T_p^2 + 1108)$ -1.5×10^{-8} $(N \times 10^{-6})^{1/3}$] J
Carrier effective mass	m_e^*	0.26 m_e
Hole effective mass	m_h^*	0.37 m_e

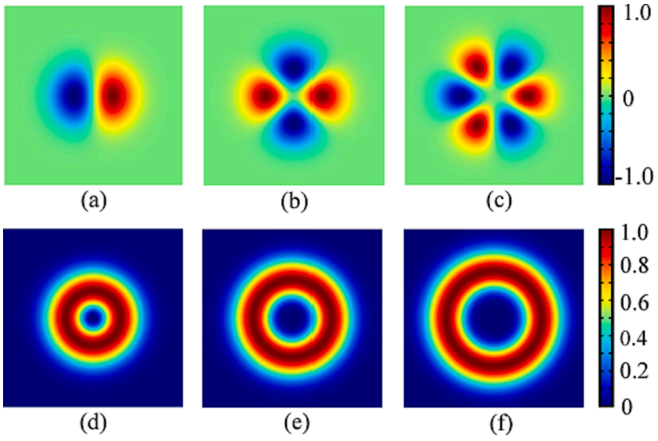

Fig. 1. The 2D spatial spots in focusing plane of femtosecond laser double-pulse vortex beam with respect to different topological charges. Pictures (a)~(c) denote the 2D electric fields spot of vortex beam for topological charges of 1 and 2 and 3. Pictures (d)~(f) display the 2D laser intensity spots of the vortex beam for the corresponding topological charge 1, 2 and 3, respectively.

2D spatial spot distribution characteristics at the focusing plane. It is observed that the 2D electric field spot can be distinctly characterized as dipolar, quadrupole and hexapole shapes for topological charges 1, 2 and 3, respectively. This is due to the tunable periodicity of the electric field around the circumference of the vortex beam by changing the topological charge. In fact, for a topological charge of 1, one spatial period of the electric field can be found around the circumference in the focus plane of the vortex beam, as shown in Fig. 1(a). However, when the integral topological charge is increased to 2 or 3, the perimetrical period of the electric field spot abruptly increases at the focusing plane, resulting in the quadrupole and hexapole profiles observed in Fig.(b) and (c). Additionally, the 2D laser intensity spot of the vortex beam typically exhibits an annular profile at topological charges of 1, 2 and 3 [(d)~(f)]. The radius of the laser intensity circle of a vortex beam increases as the topological charge is enlarged, following the scale law of $\sim l^{1/2}$, written as $r_p = \sqrt{\frac{l}{2}} w_0$. It's important to note that the annular profile of the laser intensity spot at the focusing plane exhibits spatial asymmetry in the inner and outer parts of the vortex beam ring. This has sparked interest in exploring the ultrafast dynamics of vortical thermalization in spatio-temporal regimes for potential applications in femtosecond laser nanomanufacturing, STED imaging and spectrum analysis.

The transient reflectivity at the photo-ionized surface of a silicon wafer excited by a femtosecond laser double-pulse vortex beam is shown in Fig. 2. The surface reflectivity exhibits dual-valley shapes at specific times corresponding to the peaks of the double-pulse vortex beam. Importantly, the surface reflectivity at the bright edge of the vortex beam is reduced by at least 10 % for the second vortex pulse compared to a 4 % reduction for first vortex pulse [Fig. 2a]. This indicates that the dynamic absorption of laser energy at the second pulse peak of vortex beam can be effectively enhanced via introducing a double-pulse vortex beam. In Fig. 2(b), we can see that a similar dual-valley profile of surface reflectivity is typically maintained, but the circle radius of reflectivity (r_p), defined by the distance from the center to the reflectivity valley of the vortex beam is significantly increased for the topological charge of 2 compared to the topological charge of 1. Moreover, it is evident that the circle radius of surface reflectivity decreases as reducing the topological charge of the vortex beam for different spot sizes of 12 μm, 13 μm and 15 μm [Fig. 2(c)]. This result is particularly accurate when using a smaller Gaussian spot size to achieve high-spatial resolution for annular energy pouring into silicon. This can be achieved by applying a small topological charge of a high-focused vortex beam, typically with an integral value of 1.

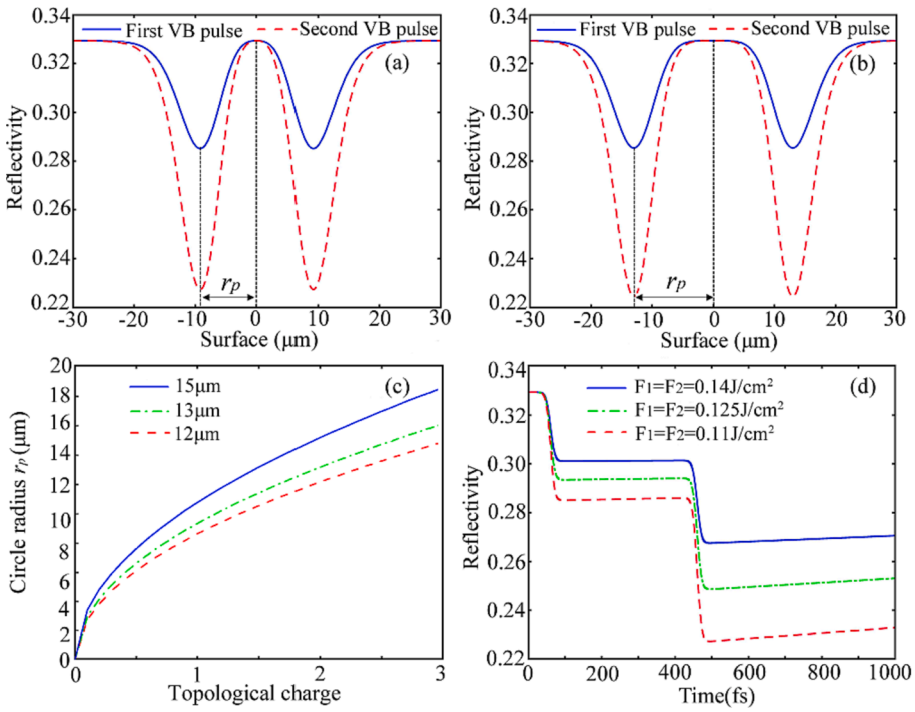

Fig. 2. The transient reflectivity at the photo-ionized surface of a silicon wafer when excited by a femtosecond laser double-pulse vortex beam. The laser wavelength is centered at 800 nm, with a pulse duration of 30 fs, and a temporal separation of 400 fs for the double-pulse vortex beam. The laser fluence of the double-pulse vortex beam is $F_1 = F_2 = 0.14$ J/cm^2. (a) Transient reflectivity of a double-pulse vortex beam with topological charge 1; (b) Transient reflectivity of a double-pulse vortex beam with topological charge 1; (c) The circle radius of transient reflectivity vs. topological charge of vortex beam; (d) The temporal evolutions of surface reflectivity. Here, VB is the abbreviation for Vortex Beam.

For example, a double-pulse configuration with a small topological charge can be highly beneficial in facilitating enhanced laser energy deposition with high-spatial resolution during the vortical thermalization dynamics in the silicon wafer. Fig. 2(d) shows the temporal evolutions of surface reflectivity at the bright edge of the vortex beam for different laser fluences of the vortex beam. The transient reflectivity is observed to decrease in a two-step fashion for fluences of 0.11 J/cm^2, 0.125 J/cm^2 and 0.14 J/cm^2. This reduction is attributed to the unique dynamics of double-pulse irradiation, which causes an abrupt decrease in reflectivity upon the arrival of respective pulse of the double-pulse vortex beam, especially for the second vortex beam pulse. This reflectivity reduction will trigger the laser energy deposition and the special traits of vortical thermalization in the silicon wafer, which will be further investigated in the following sections.

The dynamic evolution of the 2D carrier density distribution in silicon wafers excited by a femtosecond laser double-pulse vortex beam is depicted in Fig. 3. After the termination of the first vortex pulse at 30 fs, the silicon wafer is locally ionized producing an initial seed carrier in the skin layer of the silicon wafer [Fig. 3a]. A significantly multiplied carrier density can be observed especially at the bright edge of the vortex beam following the termination of the second vortex pulse at 430 fs [Fig. 3b]. In fact, the first vortex beam pulse plays a key role in pre-exciting the target, and then the second vortex beam pulse interacts with the pre-excited state, resulting in enhanced absorption of total laser energy, as typically observed in our simulation. As a result, the ionization dynamics are dramatically engaged, leading to a significant multiplication of carrier density following the double-pulse vortex pulse irradiation. Over time, the carrier density sharply reduces as a result of the Auger recombination dynamics at 3 ps [Fig. 3c]. The carrier density in the photo-ionized region of the silicon target will continuously decrease due to sustained Auger recombination dynamics until the carriers in the silicon conduction band are mostly depleted at 6 ps [see Fig. 3d]. The profiles of carrier density on the surface of the photo-excited silicon wafer following the ends of respective pulse irradiations with a double-

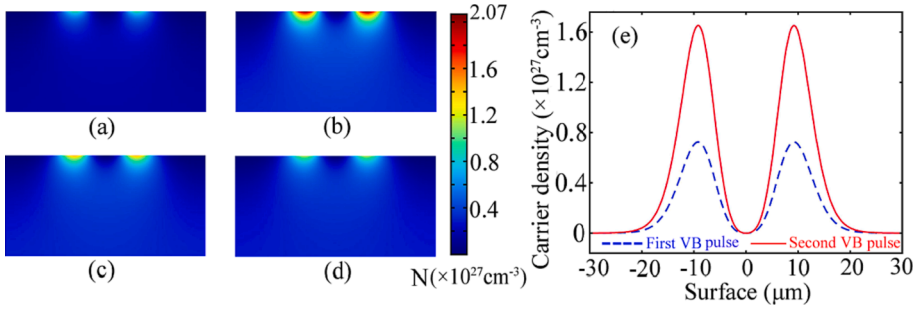

Fig. 3. The dynamic evolution of the 2D carrier density distribution in a silicon wafer when excited by a femtosecond laser double-pulse vortex beam. The laser fluence of the double-pulse vortex beam is $F_1 = F_2 = 0.14$ J/cm^2, with a wavelength centered at 800 nm and a pulse duration of 30 fs. The temporal separation of the double-pulse vortex beam is 400 fs. The different evolution times are as follows: (a) t = 30 fs; (b) t = 430 fs; (c) t = 3 ps; (d) t = 6 ps. Additionally, (e) shows the surface profile of the carrier density at the surface of the photo-excited silicon wafer.

pulse vortex beam are plotted in Fig. 3(e). It is evident that the maximum carrier density for the second vortex pulse irradiation in the photo-ionized surface region at the bright edge of the vortex beam is obviously risen compared to the first vortex pulse. The reduced reflectivity of the second vortex pulse compared to the first one, causes a significant increase in laser energy deposition and a subsequent rise in carrier density. However, in the dark center of the surface region of the vortex beam, the silicon wafer experiences less perturbation during photo-excitation and recombination relaxation due to weak transversal diffusion in contrast to the strong longitudinal diffusion of carriers in the photo-ionized region of the silicon wafer.

The dynamic evolution of the 2D temperature fields for the carrier and phonon systems of a photo-ionized silicon wafer excited by a femtosecond laser double-pulse vortex beam is shown in Fig. 4. The carrier temperature field exhibits an annular profile at the sub-surface layer of the silicon wafer at 30 fs [Fig. 4(a)], which corresponds to the termination of the first vortex pulse. Over time, the annular profile becomes blurred at the sub-surface layer of the silicon wafer at 60 fs [Fig. 4b]. Carrier thermal diffusion plays a key role in blurring the annular profile of the temperature field at sub-picosecond timescales. As a result, the annular-shaped area of the carrier temperature field is increasingly degraded at the sub-surface layer of the silicon wafer at 90 fs and 120 fs [Fig. 4(c) and (d)]. Interestingly, we observed that the silicon wafer in the sub-surface region experiences reheating, causing a sharp increase in carrier temperature at the bright edge of the vortex beam reaching as high as 7.1×10^3 K after the second vortex pulse ends at 430 fs [Fig. 4(e)]. Due to the dominant carrier-phonon coupling dynamics operating on a sub-picosecond timescale, the vortical carrier temperature field will undergo successive degradation at the sub-surface layer of the silicon wafer at 490 fs, 550 fs and 940 fs [Fig. 4(f),(g) and (h)]. On the another hand, the phonon system is less disturbed in the early stages following the termination of the first vortex beam at 30 fs [Fig. 4(i)]. After the termination of the second vortex beam at 430 fs, the phonon temperature exhibits observable rise [Fig. 4(j)]. With time, the vortical thermalization of phonon system can be further intensified due to the processive carrier-phonon coupling mechanism, resulting in an elevated phonon temperature with a highlighted annular profile at 550 fs [Fig. 4(k)]. Eventually, the carrier and phonon reach thermal equilibrium in the silicon wafer, resulting in uniform carrier and phonon temperatures across the silicon wafer at 940 fs [Fig. 4 (l)]. After thermal equilibrium, normal Fourier heat diffusion will dominate subsequent vortical thermalization until the thermal energy dissipation is completed in the silicon wafer.

The 2D temperature field evolutions for a photo-excited silicon wafer at the carrier-phonon equilibrium state, with different topological charges, is shown in Fig. 5. The temperature field typically exhibits a ring profile hollowed by a dark region in the center of the vortex beam for topological charges 1, 2, and 3, respectively [Fig. 5a, b and c]. Specifically, for a topological charge of $l = 1$, which is the case for most vortex beam applications, the ring radius of the temperature field is substantially reduced, resulting in a very small dark region in the center of the vortex beam [Fig. 5a]. However, when the topological charge is changed to $l = 2$, the ring radius of the temperature field correspondingly enlarges, causing an observable dark region in the sub-surface of the silicon wafer [Fig. 5b]. This expansion of the dark region further increases for a topological charge of $l = 3$ [Fig. 5c]. The surface temperature profile of the silicon wafer is also shown in Fig. 5d. It demonstrates that the maximal temperature at the brightest ring remains unchanged, despite the hollow dark region enlarging as the integral topological charges increase from 1 to 3.

The carrier-phonon coupling dynamics play a critical role in regulating the thermalization of vortical heating for silicon wafers. Understanding the dynamic modulations of the carrier-phonon coupling factor with respect to double-pulse vortex beam excitation is particularly important. The temporal evolutions of the carrier-phonon coupling factor for photo-excited silicon wafers with different laser fluences of a double-pulse vortex beam are shown in Fig. 6. The carrier-phonon coupling factor is extracted at the bright edge of the vortex beam on the silicon wafer surface. From Fig. 6(a), it is evident that the carrier-phonon coupling factor rapidly increases with time after the first vortex pulse excitation at 30 fs. The, the carrier-phonon coupling factor decreases slowly due to weak Auger recombination during the early stages of photo-excitation dynamics. However, the carrier-phonon coupling factor exhibits abrupt rises again after the arrival of the second vortex pulse at 430 fs. Additionally, a higher laser fluence of 0.14 J/cm^2 from the vortex beam leads to an increase in the carrier-phonon coupling factor in the photo-excited silicon wafer. Importantly, the carrier-phonon coupling factor is significantly elevated after the second pulse irradiation compared to the first vortex pulse. The result can be attributed to the intensified photo-ionization dynamics caused by the second vortex pulse which produces an abundant carrier. This in turn, amplifies the carrier-phonon coupling dynamics when a higher laser fluence of the vortex beam is applied. It is further observed that the carrier-phonon coupling factor exhibits a near-linear increase with increasing carrier density as shown in Fig. 6(b). In fact, the carrier-phonon coupling factor can be significantly amplified by employing

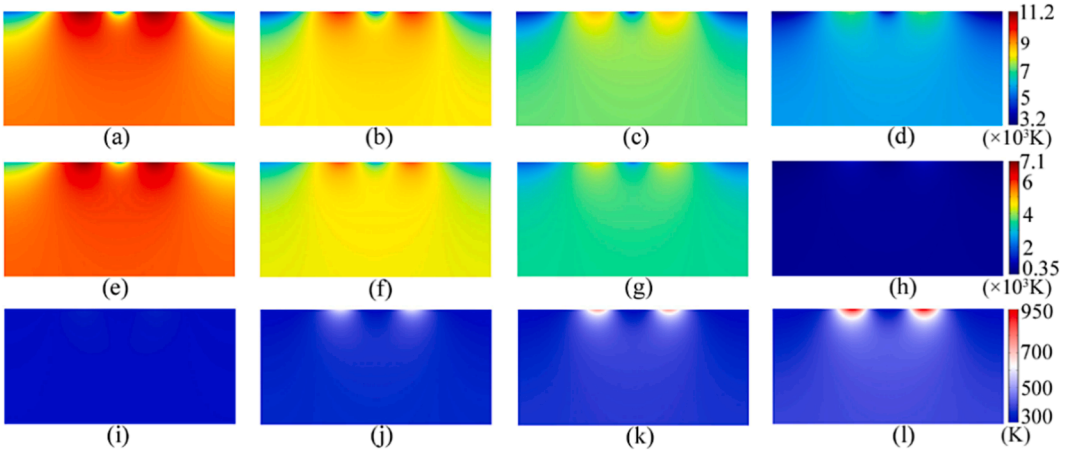

Fig. 4. shows the dynamic evolution of 2-D temperature fields for the carrier and phonon systems of a photo-ionized silicon wafer excited by a femtosecond laser double-pulse vortex beam. The laser wavelength is centered at 800 nm, with a pulse duration of 30 fs, and a temporal separation of 400 fs for the double-pulse vortex beam. The fluence of the double-pulse vortex beam is set at $F_1 = F_2 = 0.13$ J/cm^2, and the topological charge of the vortex beam is 1. The carrier temperature is shown at different evolution times: (a) t = 30 fs, (b) t = 60 fs, (c) t = 90 fs, (d) t = 120 fs, (e) t = 430 fs, (f) t = 490 fs, (g) t = 550 fs and (h) t = 940 fs. The phonon temperature is shown at different evolution times: (i) t = 30 fs, (j) t = 430 fs, (k) t = 550 fs and (l) t = 940 fs.

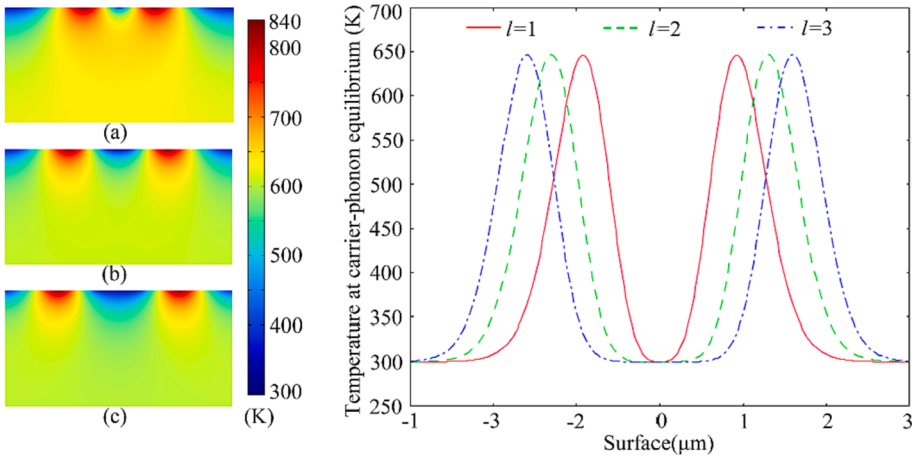

Fig. 5. The 2D temperature field evolutions for photo-excited silicon wafer at the carrier-phonon equilibrium state in term of different topological charges. The laser wavelength is centered at 800 nm, with a pulse duration of 30 fs, and a temporal separation of 400 fs for the double-pulse vortex beam. The fluence of the double-pulse vortex beam is set at $F_1 = F_2 = 0.1$ J/cm^2.

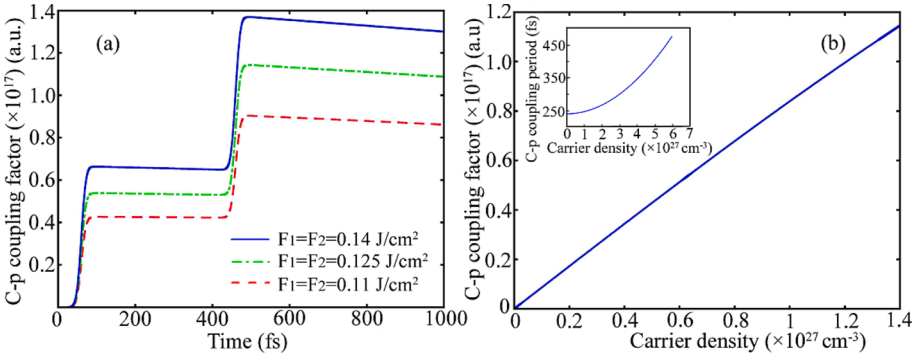

Fig. 6. The temporal evolution of the carrier-phonon coupling factor for a photo-excited silicon wafer at different laser fluences of a double-pulse vortex beam. The laser wavelength is centered at 800 nm, with a pulse duration of 30 fs and a temporal separation of 400 fs for the double-pulse vortex beam. The topological charge of the vortex beam is taken as $l = 1$. (a) The graph depicts the carrier-phonon coupling factor as a function of evolution time; (b) The graph shows the carrier-phonon coupling factor plotted against carrier density.

the femtosecond laser double-pulse vortex beam, leading to a prolonged carrier-phonon coupling period as seen in the inset of Fig. 6(b). This could potentially cause the an extended heating cycle for phonon vortical thermalization in a silicon wafer.

Fig. 7 shows the changes in the carrier-phonon coupling factor and the resulting vortical thermalization in the silicon wafer as a function of the laser fluence of the double-pulse vortex beam. The carrier-phonon coupling factor is determined at a time following terminations of each pulse irradiations of the double-pulse vortex beam. The results indicate that the carrier-phonon coupling factor increases notably as the laser fluence of the vortex beam increases, particularly after the second pulse irradiation. We can observe that compared to first vortex pulse, more than 2 times improvement in the carrier-phonon coupling factor can be definitely achieved after the second vortex pulse at a larger fluence of 0.14 J/cm^2. This indicates that the second vortex pulse practically plays a crucial role in amplifying the carrier-phonon coupling dynamics for

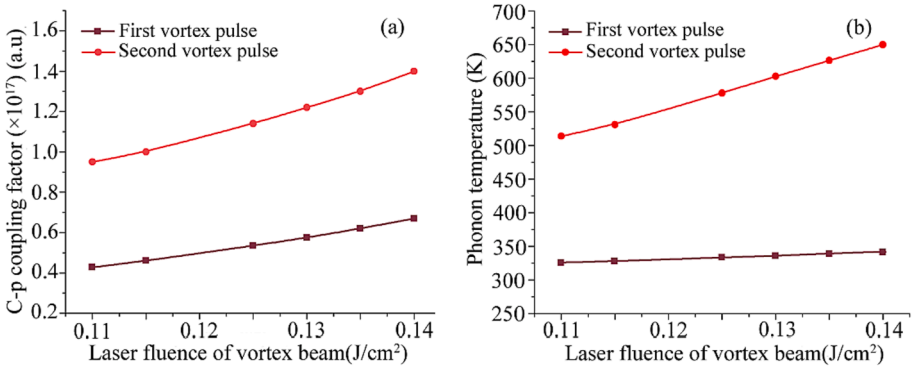

Fig. 7. The modifications of the carrier-phonon coupling factor and the resulting vortical thermalization in the silicon wafer. These changes are plotted against as a function of the laser fluence of the double-pulse vortex beam. The laser wavelength is centered at 800 nm, the pulse duration is 30 fs, and the temporal separation of the double-pulse vortex beam is 400 fs.

silicon vortical thermalization, especially at higher laser fluence [Fig. 7a]. In fact, the first vortex pulse acts as a pre-ionization role, facilitating reduced reflectivity and enhanced dynamics of laser absorption. Simultaneously the second vortex pulse amplifies the carrier-phonon coupling factor to intensify the vortical thermalization dynamics of the phonon system.

As a result, the phonon temperature rises rapidly after the second vortex pulse irradiation, especially at higher larger fluence of the double-pulse vortex beam [Fig. 7(b)]. It is important to note that the vortical thermalization dynamics in the silicon wafer will ultimately terminate in a period of 940 fs, while carrier recombination can occur following the Auger recombination dynamics at 6 fs. These results provide a basic understanding of vortical thermalization in silicon wafer targets under femtosecond laser double-pulse vortex beam irradiation, putting forward the feasibility of advanced applications such as STED imaging, ultrafast SERS sensing and laser fabrication of sophisticated structures, etc.

3. Conclusions

We conducted a theoretical investigation into the ultrafast thermalization dynamics in a silicon wafer when excited by a femtosecond laser double-pulse vortex beam. It is observed that the silicon target can be vortically thermalized by employing the double-pulse vortex beam irradiation. We also discovered that the double-pulse laser energy deposition on the silicon wafer is significantly increased due to the dynamically reduced transient reflectivity. This unprecedented enhancement helps to explain the early mechanism for intensifying the vortical thermalization dynamics. Specifically, our research revealed that the double-pulse vortex beam plays a crucial role in amplifying the carrier-phonon coupling dynamics, resulting in a more than 2-fold enhancement of the carrier-phonon coupling factor. This ultimately facilitates the vortical thermalization of the phonon system in the picosecond time regime. This study paves the way for in-depth understanding of the fundamental dynamics of femtosecond laser double-pulse heating of semiconductors, which could potentially benefit advanced applications such as vortex beam imaging of STED, ultrafast SERS sensing and laser fabrication of sophisticated structures, etc.

CRediT authorship contribution statement

Guangqing Du: Conceptualization, Writing – original draft, Writing – review & editing. **Fangrui Yu:** Data curation, Investigation, Software. **Ahmad Waqas:** Formal analysis, Writing – review & editing. **Feng Chen:** Funding acquisition, Supervision.

Declaration of Competing Interest

The authors declare that they have no known competing financial interests or personal relationships that could have appeared to influence the work reported in this paper.

Data availability

Data will be made available on request.

Acknowledgement

This work is supported by the National Science Foundation of China under the Grant nos. 12127806, 62175195, the International Joint Research Laboratory for Micro/Nano Manufacturing and Measurement Technologies.

References

[1] B.L. Liao, A.A. Maznev, K.A. Nelson, G. Chen, Photo-excited charge carriers suppress sub-terahertz phonon mode in silicon at room temperature, Nat. Commun. 7 (2016) 13174.
[2] J.G. Li, R.D. Yang, Y. Rho, P.H. Ci, M. Eliceiri, H.K. Park, J.Q. Wu, C. P. Grigoropoulos, Ultrafast optical nanoscopy of carrier dynamics in silicon nanowires, Nano Lett. 23 (2023) 1445–1450.
[3] M. Chanal, V.Y. Fedorov, M. Chambonneau, R. Clady, S. Tzortzakis, D. Grojo, Crossing the threshold of ultrafast laser writing in bulk silicon, Nat. Commun. 8 (2017) 773.
[4] E. Allahyari, J.J.J. Nivas, E. Skoulas, R. Bruzzese, G.D. Tsibidis, E. Stratakis, S. Amoruso, On the formation and features of the supra-wavelength grooves generated during femtosecond laser surface structuring of silicon, Appl. Surf. Sci. 528 (2020) 146607.
[5] E. Najafi, V. Ivanov, A. Zewail, M. Bernardi, Super diffusion of excited carriers in semiconductors, Super-diffusion of excited carriers in semiconductors, Nat. Commun. 8 (2017) 15177.
[6] M. Spyridaki, E. Koudoumas, P. Tzanetakis, C. Fotakis, R. Stoian, A. Rosenfeld, I. V. Hertel, Temporal pulse manipulation and ion generation in ultrafast laser ablation of silicon, Appl. Phys. Lett. 83 (2003) 7.
[7] X.M. Lin, X.H. Li, Y.B. Zhang, Y.X. Hou, X.Y. Liu, C.F. Deng, Q. Zhou, Third harmonic generation on silicon surface induced by femtosecond laser, Opt. Laser Technol. 111 (2019) 255–261.
[8] Y. Levy, T.-J.-Y. Derrien, N.M. Bulgakova, E.L. Gurevich, T. Mocek, Relaxation dynamics of femtosecond-laser-induced temperature modulation on the surfaces of metals and semiconductors, Appl. Surf. Sci. 374 (2016) 157–164.
[9] A.J. Sabbah, D.M. Riffe, Femtosecond pump-probe reflectivity study of silicon carrier dynamics, Phys. Rev. B 66 (2002) 165217.
[10] D.P. Korfiatis, K.-A.-T. Thoma, J.C. Vardaxoglou, Numerical modeling of ultrashort-pulse laser ablation of silicon, Appl. Surf. Sci. 255 (2009) 7605–7609.
[11] T. Feng, G. Chen, H.N. Han, J. Qiao, Femtosecond-laser-ablation dynamics in silicon revealed by transient reflectivity change, Micromachines 13 (2022) 14.
[12] M.G. Rahimian, A. Jain, H. Larocque, P.B. Corkum, E. Karimi, V.R. Bhardwaj, Spatially controlled nano-structuring of silicon with femtosecond vortex pulses, Sci. Rep. 10 (2020) 12643.
[13] J.C. Ni, C.W. Wang, C.C. Zhang, Y.L. Hu, L. Yang, Z.X. Lao, B. Xu, J.W. Li, D. Wu, J. R. Chu, Three-dimensional chiral microstructures fabricated by structured optical vortices in isotropic material, Light Sci. Appl. 6 (2017) e17011.
[14] Y. Tang, W. Perrie, D.R. Sierra, Q.L. Li, D. Liu, S.P. Edwardson, G. Dearden, Laser–material interactions of high-quality ultrashort pulsed vector vortex beams, Micromachines 12 (2021) 376.
[15] M.G. Rahimian, F. Bouchard, H. Al-Khazraji, E. Karimi, P.B. Corkum, V. R. Bhardwaj, Polarization dependent nanostructuring of silicon with femtosecond vortex pulse, APL Photonics 2 (2017) 086104.
[16] N. Tian, L. Fu, M. Gu, Resolution and contrast enhancement of subtractive second harmonic generation microscopy with a circularly polarized vortex beam, Sci. Rep. 5 (2015) 13580.
[17] J.J.J. Nivas, S.T. He, Z.M. Song, A. Rubano, A. Vecchione, D. Paparo, L. Marrucci, R. Bruzzese, S. Amoruso, Femtosecond laser surface structuring of silicon with Gaussian and optical vortex beams, Appl. Surf. Sci. 418 (2017) 565–571.
[18] H.C. Cheng, P. Li, S. Liu, P. Chen, L. Han, Y. Zhang, W. Hu, J.L. Zhao, Vortex-controlled morphology conversion of microstructures on silicon induced by femtosecond vector vortex beams, Appl. Phys. Lett. 111 (2017) 141901.
[19] F. Fraggelakis, G. Mincuzzi, J. Lopez, I. Manek-Hönninger, R. Kling, Controlling 2D laser nano structuring over large area with double femtosecond pulses, Appl. Surf. Sci. 470 (2019) 677–686.
[20] X.Y. Sun, K.F. Cheng, D.K. Chu, Y.W. Hu, Z.L. Dong, J.A. Duan, Controlling of surface ablation threshold of fused silica by double-pulsed femtosecond laser, Appl. Phys. A 126 (2020) 698.
[21] C.J. Pan, Q.S. Wang, J.Y. Sun, F.F. Wang, J.X. Sun, G.Y. Wang, Y.F. Lu, L. Jiang, Dynamics and its modulation of laser-induced plasma and shockwave in femtosecond double pulse ablation of silicon, Appl. Phys. Express 13 (2020) 012006.
[22] M.E. Povarnitsyn, T.E. Itina, K.V. Khishchenko, P.R. Levashov, Suppression of ablation in femtosecond double-Pulse experiments, Phys. Rev. Lett. 103 (2009) 195002.
[23] L. Stoyanov, A. Stefanov, A. Dreischuh, G.G. Paulus, Gouy phase of Bessel-Gaussian beams: theory vs. experiment, Opt. Express 31 (2023) 13683–13699.
[24] R. Uren, S. Beecher, C.R. Smith, W.A. Clarkson, Method for generating high purity Laguerre-Gaussian vortex modes, IEEE J. Quantum Elect. 55 (2019) 1700109.
[25] K. Sokolowski-Tinten, D. von der Linde, Generation of dense electron-hole plasmas in silicon, Phys. Rev. B 61 (2000) 4.
[26] H.M. van Driel, Kinetics of high-density plasmas generated in Si by 1.06- and 0.53-pm picosecond laser pulses, Phys. Rev. B 35 (1987) 15.
[27] T.-J.-Y. Derrien, J. Krüger, T.E. Itina, S. Höhm, A. Rosenfeld, J. Bonse, Rippled area formed by surface plasmon polaritons upon femtosecond laser double-pulse irradiation of silicon: the role of carrier generation and relaxation processes, Appl. Phys. A 117 (2014) 77–81.
[28] T.J.Y. Derrien, T.E. Itina, R. Torres, T. Sarnet, M. Sentis, Possible surface plasmon polariton excitation under femtosecond laser irradiation of silicon, J. Appl. Phys. 114 (2013) 083104.
[29] A. Ramer, O. Osmani, B. Rethfeld, Laser damage in silicon: Energy absorption, relaxation, and transport, J. Appl. Phys. 116 (2014) 053508.